Paper presented at the SPIE Medical Imaging meeting, Ultrasonic Imaging and Signal Processing, 2002:

# Comparison Between Different Encoding Schemes for Synthetic Aperture Imaging

Svetoslav Ivanov Nikolov, (sn@oersted.dtu.dk) and Jørgen Arendt Jensen (jaj@oersted.dtu.dk),
Center for Fast Ultrasound Imaging,
Ørsted•DTU, Bldg. 348,
Technical University of Denmark,
DK-2800 Lyngby, Denmark

Proceedings of SPIE, Eds. M. F. Insana and W. Walker, 2002.
http://proceedings.spiedigitallibrary.org/proceeding.aspx?articleid=880554

```
@inbook{ref_nikolov_jensen_2002a,
  title     = "Comparison between different encoding schemes for synthetic aperture imaging",
  author    = "Svetoslav Nikolov and Jensen, {Jørgen Arendt}",
  year      = "2002",
  pages     = "1-12",
  booktitle = "Proc. SPIE - Progress in biomedical optics and imaging",
}
```

# Comparison Between Different Encoding Schemes for Synthetic Aperture Imaging

Svetoslav I. Nikolov and Jørgen A. Jensen
Center for Fast Ultrasound Imaging, Ørsted•DTU, Bldg. 348,
Technical University of Denmark, DK-2800, Kgs. Lyngby, Denmark

## ABSTRACT

Synthetic transmit aperture ultrasound (STAU) imaging can create images with as low as 2 emissions, making it attractive for 3D real-time imaging. Two are the major problems to be solved: (1) complexity of the hardware involved, and (2) poor image quality due to low signal to noise ratio (SNR). We have solved the first problem by building a scanner capable of acquiring data using STAU in real-time. The SNR is increased by using encoded signals, which make it possible to send more energy in the body, while preserving the spatial and contrast resolution.

The performance of temporal, spatial and spatio-temporal encoding was investigated. Experiments on wire phantom in water were carried out to quantify the gain from the different encodings. The gain in SNR using an FM modulated pulse is 12 dB.

The penetration depth of the images was studied using tissue mimicking phantom with frequency dependent attenuation of 0.5 dB/(cm MHz). The combination of spatial and temporal encoding have highest penetration depth. Images to a depth of 110 mm, can successfully be made with contrast resolution comparable to that of a linear array image.

The in-vivo scans show that the motion artifacts do not significantly influence the performance of the STAU.

**Keywords:** synthetic aperture, ultrasound, focusing, imaging, temporal coding, spatial coding, coding

## 1. INTRODUCTION

Synthetic Aperture Ultrasound imaging (SAU) has been studied for more than two decades now. Various advantages of SAU compared to the conventional ultrasound imaging were explored: (a) simpler electronic front end;[1–4] (b) better image quality;[5,6] (c) fast imaging, applicable for real-time three-dimensional scanning;[7,8] (d) estimation of low blood flow and high frame rate of color flow mapping.[9,10] In spite all of the investigations, such systems are still not in clinical use. Among the problems are: (a) the presence of motion artifacts,[3,4] and (b) a low Signal-to-Noise Ratio (SNR).[7,11]

We have previously shown how to compensate for the motion artifacts,[10,12] and how to avoid their effect in blood flow estimations.[9,10] Various coding schemes have been suggested to increase the SNR: temporal encoding,[13] spatial encoding,[14] and their combination.[15] Some of these methods have been investigated only in simulation, some tried *in-vivo*, but not with SAU. At the Center for Fast Ultrasound Imaging (CFU), a scanner capable of implementing any of the aforementioned encoding schemes for SAU in real time was developed.[16]

The purpose of this paper is to experimentally investigate the increase in SNR using the various spatial and temporal encoding schemes. The comparison is done on data measured on phantoms. The performance of the algorithms is also shown for different imaging situations *in-vivo*.

## 2. THEORY

In this section the theory behind the SAU imaging is presented. At the present state of technology, the system complexity is not of major concern, and the focus is put on Synthetic *Transmit* Aperture Ultrasound imaging (STAU).

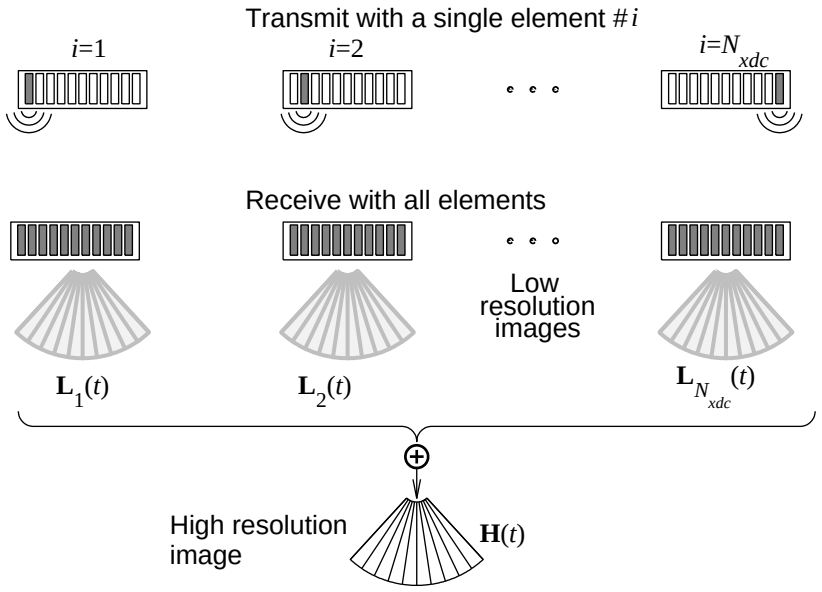


Figure 1. Synthetic transmit aperture imaging.

### 2.1 Synthetic Transmit Aperture Imaging

Synthetic transmit aperture imaging (STAU) is done by sending out a waveform which propagates through all of the scanned region, and whose wavefront is known. Such waves are either spherical or plane. Although plane waves have been also used for STAU imaging,[17] the use of spherical waves has been more widely investigated. A nearly spherical* wave can be created by either transmitting with a single element, or by using multiple elements,[2,7,8] the delays of which are appropriately set. The point to which the origin of such a wave can be traced, will be called a "virtual" source element.[10] In the case that only a single element is used in transmit, the positions of the virtual and real source coincide.

Figure 1 illustrates the process of creating a synthetic aperture image, when only a single element is used in transmission. The wave created by a single element is spherical, and propagates through whole region of interest. The back scattered echoes carry information from all directions, and by applying different delays on the received signals a scan line can be formed in *any* direction. To speed up the acquisition, scan lines in *all* directions are formed, thus creating a whole image. Since the image is focused only in receive, it has a low resolution, hence the name *Low Resolution Image* (LRI). The beamforming of a single line $L_{il}(t)$ is:

$$L_{il}(t) = \sum_{j=1}^{N_{xdc}} a_{lij}(t) r_{ij}(\tau_{lij}(t)), \tag{1}$$

where $r_{ij}(t)$ is the Radio Frequency (RF) signal received by the element $j$ , after transmitting with element $i$, and $\tau_{lij}(t)$ is the round-trip propagation time from element $i$ to the current focal point and back to element $j$. It is a function of $t$, which is the time from the trigger of the emission. The apodization coefficient $a_{lij}$ can also be a function of $t$. The subscript $l$ is used to index the scan lines comprising the LRI. LRI in matrix form is written as:

$$\mathbf{L}_i(t) = [L_{i1}(t), L_{i2}(t), \cdots, L_{iN_l}(t)], \tag{2}$$

where $N_l$ is the number of scan lines. The columns of the matrix correspond to different image directions, and the rows correspond to samples in depth. After transmitting with the first element $i = 1$, a second element is used in transmit $i = 2$. The RF signals in $\mathbf{L}_1(t)$ and $\mathbf{L}_2(2)$, although focused at the same points, have different

*Strictly speaking the wave has a complex shape determined by the geometry of the transducer elements.

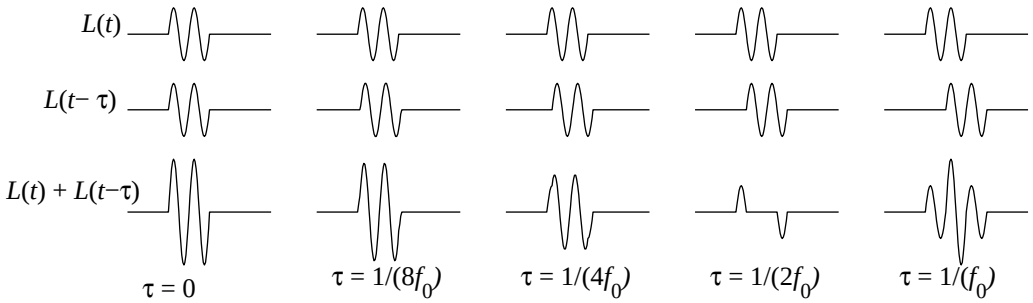


Figure 2. Illustration of several cases of motion artifacts

| Vessel | Scan plane | Motion | $v_{max}$ |
|---|---|---|---|
| Carotid artery | Transverse, scan angle 90° | P, B | $8.9 \cdot 10^{-3}$ m/s |
| Hepatic vein | Right liver lobe, intercostal scan | B, H (P) | $6.2 \cdot 10^{-3}$ m/s |
| Hepatic vein | Right liver lobe, intercostal scan | H (P) | $4.2 \cdot 10^{-3}$ m/s |
| Hepatic vein | Left liver lobe, epigastric scan | H (P) | $10.1 \cdot 10^{-3}$ m/s |

Table 1. Maximum velocities of the vessel walls due to pulsation (P), heart beat (H), and breathing (B). Data published by Schlaikjer et. al.[18]

phases due to the different origins of the sources. Summing them is equivalent to focusing in transmit. Because the focusing was done on every point, this is equivalent to dynamic transmit focusing. After using all of the elements across the aperture, a High Resolution Image (HRI) can be made by summing the low resolution ones:

$$\mathbf{H}(t) = \sum_{i=1}^{N_{xdc}} \mathbf{L}_i(t). \tag{3}$$

It is possible to reduce the number of emissions by using only some of the transducer elements.[7,8,14] The number of emissions will be further denoted by $N_{xmt}$. The resolution of $\mathbf{H}(t)$ is determined by the distance between the outermost elements, and the side- and grating-lobes level by the number of emissions $N_{xmt}$. The larger the number of emissions $N_{xmt}$, the lower the side lobe energy is. The acquisition time is, however, increased, and the image is more susceptible to motion artifacts, which are discussed in the next section.

## 2.2 Motion Artifacts

In order to create a HRI the low resolution images should be summed coherently. The motion of the scatterers between two transmissions prohibits this summation as shown in Fig. 2.2. From the figure it can be seen that there are certain tolerance intervals for the motion. The worst case is when the scatterers move at a distance $\lambda/2$ between every two emissions since that results in destructive interference. If the motion for the $N_{xmt}$ emissions is less than $\lambda/2$, then the sum of the signals will still be larger than the individual RF traces, and the end image will be focused. Assuming a speed of sound $c = 1500$ m/s, center frequency $f_0 = 5$ MHz, a pulse repetition frequency of $f_{prf} = 5$ kHz, and $N_{xmt} = 60$, the maximum velocity for which the time shift is less than half a period is:

$$v_{max} < \frac{f_{prf} c}{4 f_0 N_{xmt}} = \frac{5 \cdot 10^3 \cdot 15 \cdot 10^2}{4 \cdot 5 \cdot 10^6 \cdot 60} = 6.3 \cdot 10^{-3} \text{ m/s} \tag{4}$$

The major causes of motion are the heart beat, pulsation, and breathing.[18] The motion, apart from the heart, is most pronounced at the walls of the blood vessels. Table 2.2 shows the maximum velocity $v_{max}$ of the vessel walls for some of the blood vessels in the presence of different causes of motion. It can be seen that the peak velocities in the investigated regions are bigger than $v_{max}$ found in (4). In many cases (such as scanning the carotid artery) either a higher $f_{prf}$ or a lower $f_0$ will be used. The number of emissions $N_{xmt}$ can also be reduced.

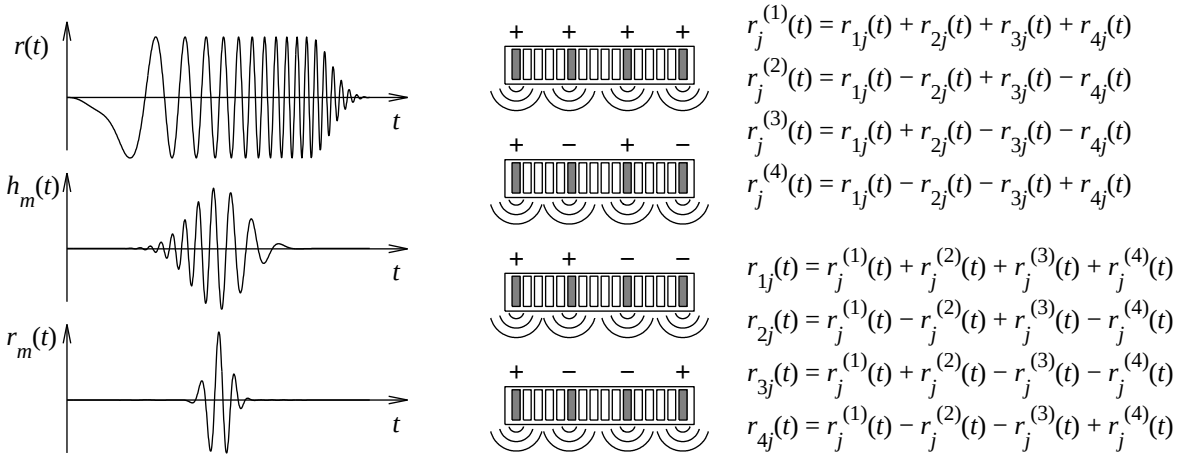


**(a)** From top to bottom: the received signal, the compression filter, and the result of the compression.

**(b)** The apodization in transmit is given with '+' and '-'. $r_j^{(n)}(t)$ is the signal received by element $j$ at emission $n$. $r_{ij}(t)$ is the part of the signal that is transmitted by element $i$ and received by element $j$.

Figure 3. Illustration of (a) temporal, and (b) spatial encoding.

### 2.3 Signal to Noise Ratio

The SNR is one of the major problems for STAU imaging. In receive all of the transducer elements are used, and the gain in SNR (GSNR), of the beamformed RF line due to the receive focusing is the same as in "conventional" ultrasound imaging. The noise is assumed to be white, and the SNR is increased $\sqrt{N_{rcv}}$ times, where $N_{rcv}$ is number of receiving elements. The degraded SNR arises from using few elements in the transmission. Many authors[2,7,11] suggest the use of multiple elements in transmit, to create a spherical wave. Usually the number of active elements rarely exceeds $N_{act} = 30$. The wave is divergent and its amplitude falls off with $1/r$, even in non-attenuating medium, ($r$ is the traveled distance). In conventional ultrasound scanning, however, a focused beam is sent into the tissue, and a much larger in amplitude signal is returned, even for the same number of transmitting elements. It is clear that to obtain the same SNR of the signal on a single channel, as many as possible of the transducer elements must be used in transmit, and each of them should send a long pulse. To maintain the lateral and axial resolutions, spatial and temporal coding must be used, respectively.

#### 2.3.1 Temporal encoding

Usually matched filtering is applied on the received signal. The peak of the signal returned by a point scatterer is determined by the maximum of the autocorrelation function of the transmitted signal, which is equal to the energy in the signal. The maximum amplitude of the transmitted signal is limited for safety reasons, and one way to increase the transmitted energy is to use either a long pulse, or a sequence of pulses. Using a long pulse, however, decreases the axial resolution, unless some form of modulation is used. The linear frequency modulated (FM) pulse (chirp), is especially suited for ultrasound imaging, since its compression properties are retained in an attenuating media.[13]

One such chirp, and the result of the filtration with a windowed matched filter, is shown in Fig. 3(a). The rising and the falling edges of the chirp are weighted in order to reduce the range side lobes. The matched filter is weighted even more. The weighting of this filter is done in such a way, as to smoothen the spectrum of the received signal.[13]

The gain in SNR (GSNR) due to mathed filtering is:

$$GSNR = \frac{SNR_{out}}{SNR_{in}} = TB. \tag{5}$$

The pulse that will be used for the experiments has a 3 cycles, Hamming weighted pulse at 7 MHz. The chirp used in the experiments has a duration $T = 20$ $\mu$s and a bandwidth of 7 MHz. The expected gain in signal-to-noise ratio is:

$$GSNR_{chirp} - GSNR_{sin} = 10(\log_{10}(20 \times 7) - \log_{10}(0.45 \times 10)) = 14.9 \text{ dB}. \tag{6}$$

However, the weighting applied on the chirp will reduce the GSNR.

Another class of temporally encoded signals, which are suitable for ultrasound imaging, is the class of binary encoded waveforms such as the Golay codes.[15] The use of Golay pairs, however, requires 2 emissions from every element position, thus increasing the acquisition time.

### 2.3.2 Spatial encoding

In order to increase the SNR, as many as possible of the transducer elements must be used in transmit. The idea is to transmit with all of the virtual sources at the same time instead of transmitting with a single virtual source at a time, as shown in Fig. 3(b). The signal received by element $j$ is a linear combination of the signals $r_{ij}(t)$ that would have been received by $j$, if the transmitting elements $i$ had transmitted one by one. At every emission, the apodization coefficients in transmit are changed. A system of linear equations is made, and when solved the individual components $r_{ij}(t)$ can be found from its solution. In matrix form the signal received by element $j$ at emission $n$, $n \in [1, N_{xmt}]$ is:

$$\begin{aligned} \vec{r}_j(t) &= \mathbf{Q}\vec{r}_{ij}(t) \\ \vec{r}_{ij}(t) &= \mathbf{Q}^{-1}\vec{r}_j(t). \end{aligned} \tag{7}$$

$\mathbf{Q}$ is the encoding matrix, which consists from the transmit apodization coefficients. The rows of $\mathbf{Q}$ correspond to the emission number $n$, and the columns to the index of transmitting element $i$. A suitable encoding matrix $\mathbf{Q}$ is the Hadamard matrix $\mathbf{H}$.[14] The Hadamard matrix is given by its order $N$, and the lowest order is $N = 2$. The matrix of order 2 is:

$$\mathbf{H}_2 = \begin{bmatrix} 1 & 1 \\ 1 & -1 \end{bmatrix} \tag{8}$$

The order of the matrix can be only an even number, and the matrix of order $2N$ is found recursively from the matrix of order $N$ by:

$$\mathbf{H}_{2N} = \begin{bmatrix} \mathbf{H}_N & \mathbf{H}_N \\ \mathbf{H}_N & -\mathbf{H}_N \end{bmatrix} \tag{9}$$

The inverse matrix is the matrix itself scaled by $1/N$:

$$\mathbf{H}_N^{-1} = \frac{1}{N}\mathbf{H}_N. \tag{10}$$

The process of coding and decoding using Hadamard matrices for $N = 4$ is given in Fig. 3(b).

### 2.3.3 Spatial and temporal encoding

There are two types of combinations of spatial and temporal encoding. The first is to use spatial encoding, and instead of a short pulse to use a long linear FM chirp. The process of beam formation is preceded by two pre-processing stages: (1) spatial decoding, and (2) pulse compression.

The second combination is to use spatial encoding in combination with orthogonal temporal signals.[15] This is used in order to decrease the number of emissions. For example, if one has two orthogonal signals $A(t)$ and $B(t)$, then the transmissions in the case of $N_{xmt} = 4$ is:

$$\begin{matrix} A_1(t) & A_2(t) & B_3(t) & B_4(t) \\ A_1(t) & -A_2(t) & B_3(t) & -B_4(t) \end{matrix}$$

In the first decoding stage, the combination of signals $A_1(t) + B_3(t)$, and $A_2(t) + B_4(t)$ are found by adding and subtracting the received signals. In the second decoding stage $A_1(t)$ and $A_2(t)$ are separated from $B_3(t)$ and $B_4$ by using cross-correlation ($A$ is orthogonal to $B$).

| Parameter name | Notation | Value | Unit |
|---|---|---|---|
| Number of receive elements | $N_{rcv}$ | 64 | - |
| Mean frequency | $f_0$ | 7.0 | MHz |
| Sampling frequency | $f_s$ | 40 | MHz |
| Resolution of A/D converter | - | 12 | bits |
| Transducer pitch | $d_x$ | 208 | $\mu$m |
| Element width | $w$ | 173 | $\mu$m |
| Element height (elevation) | $h$ | 4.5 | mm |
| Elevation focus | $F$ | 25 | mm |
| Fractional bandwidth | $BW$ | 60 | % |

Table 2. Parameters of the measurement system.

## 3. RESULTS

The various strategies will now be evaluated- Three sets of measurements were done: (a) on a wire, (b) on a phantom. and (c) in-vivo. The measurements on the wire were used to characterize the parameters of the system such as resolution, integrated side lobe to main lobe ratio (ISLMLR), and peak signal to noise ratio (PSNR). The measurements on the phantom are used to demonstrate the improved penetration depth with the use of temporal and spatial encoding, and the measurements in-vivo are used to show that the motion artifacts do not distort the image.

### 3.1 Experimental Setup

The measurements were done using the experimental system RASMUS,[16] developed at the Center for Fast Ultrasound Imaging. The system has 128 transmit channels and 64 receive channels which can be multiplexed to 128 transducer elements. Up to 4096 different transmit waveforms per channel can be set up in transmit. Each waveform can contain up-to 4096 12 bit samples. The receiver has 128 MB focusing look up tables per channel, and any delay can be set up. Additionally, 16 GB of 12 bit data sampled at 40 MHz can be stored for all the channels, for off-line processing. The transmitting and the receiving units are fully programmable and controlled by software. The parameters of the system are given in Table 2.

### 3.2 Measurements on a Wire Phantom

In order to characterize the system, a wire phantom was scanned. It consisted of 5 wires, placed along a line at 60° to the surface of the transducer. The width of the wires was 0.25 mm. B-mode images of the wire phantom are shown in Fig. 4. In the rest of the figures and tables, the abbreviation "chirp_" will be used to denote that a linear FM modulated pulse was used in transmit, and "sin_" that the used excitation is a conventional RF pulse. The prefix "had_" will show that the imaging is combined with spatially encoded transmit. The numbers added to the titles of the plots will show the number of transmit events used to form a single image. Acquisitions with 4, 8, 16, 32, and 64 firings were done for each of the transmit schemes.

The same FM pulse was used for all of the experiments. The duration of the FM pulse is $T = 20$ $\mu$s, and a bandwidth $B = 7$ MHz. The mean frequency of the chirp is 7.0 MHz. The rising and the falling edges of the chirp are weighted in order to suppress the range side lobes,[19,20] which in this case are lower than -55 dB from the peak. The RF pulse that is used for the cases designated with "sin", is a 3 cycles RF pulse at 7 MHz. The envelope of the pulse is weighted with a Hamming window.

For the cases, in which there was no spatial encoding, 25 elements were used to emulate the radiation pattern of a single element in transmit. For the cases with spatial Hadamard encoding, the number of transmit elements used to emulate the radiation pattern of a single one was: 15, 7, 3, 1, 1, for $N_{xmt}$ equal to 4, 8, 16, 32, and 64, respectively.

All of the images in Fig. 4 have a dynamic range of 60 dB, and were acquired with 64 emissions. It can be seen that the image with least imaging artifacts is the image obtained without any kind of encoding. This fact is confirmed by looking at the plots in Fig. 5, and at Table 3.

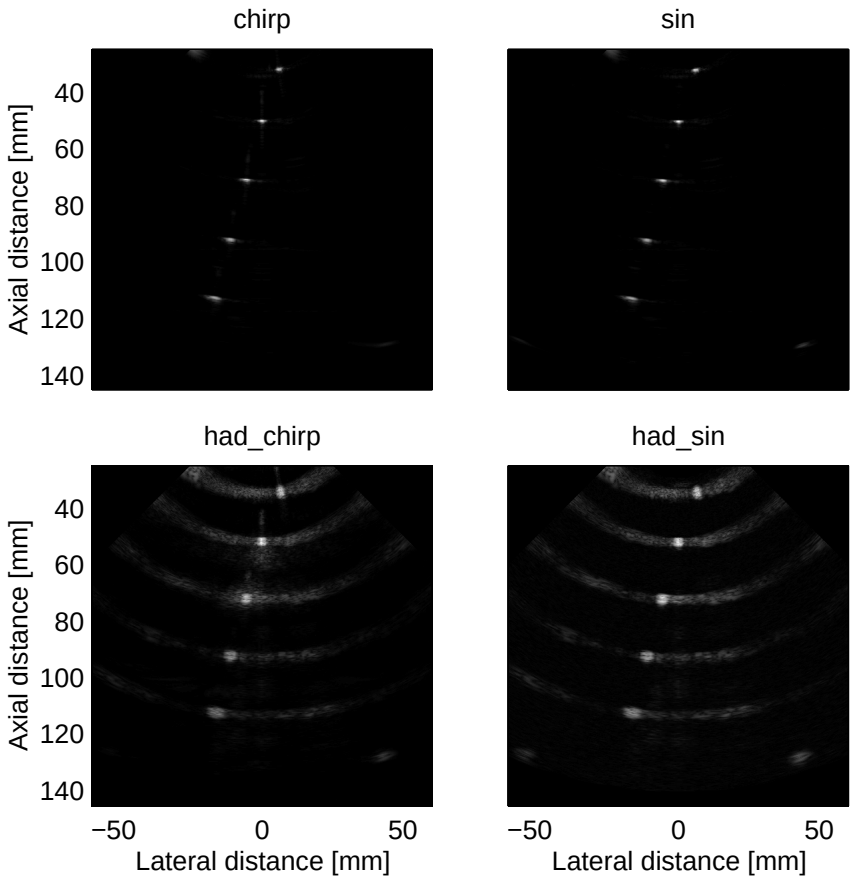


Figure 4. B-mode images of the wire phantom used to characterize the point spread function of the system.

The lower amount of the artifacts for the case without *any* encoding is due to the lack of range side lobe levels, which are present when FM modulated chirps are used. An indication for this is the slightly lower IMLSLR when chirps are used (higher side lobe energy). The IMLSLR is lowest for the scans employing Hadamard encoding. In this experiment the use of Hadamard encoding worsened the performance of the system, contrary to all expectations. The only reasonable explanation for this, is that the propagation in the water introduced non-linearities in the response, and in this way the components of the signal could not be separated properly.

The purpose of using coded excitations is to increase the signal to noise ratio. Figure 6 shows the peak signal to noise ratio for the different encoding schemes. This indicator was calculated for the point which is at 50 mm away from the focus. The actual values are given in Table 4. The highest PSNR is found only when chirps are used in transmit. The gain in SNR relative to the conventional RF pulse is approximately 12 dB. The bad PSNR, when Hadamard encoding is used, is due to the poor separation of the echoes, which results in lower peak signal. The RMS value of the noise is actually decreased, and is between 5 to 10 dB lower than for the cases without Hadamard encoding, but ratio is lower due to the poor IMLSLR.

### 3.3 Measurements on a Tissue Mimicking Phantom

The same set of measurements was carried out on a tissue mimicking phantom. The attenuation in the phantom was 0.5 dB/(cm.MHz). Figure 7 shows the result of using 64 emissions for the different encoding types. It can be seen that the case without any encoding performs worst. It has low penetration depth (the row of point scatterers at depth of 82 mm cannot be seen), and worse focusing. The use of Hadamard encoding in transmit improves the focusing abilities of the system, and somewhat the penetration depth. A significant increase in the contrast of the image and the penetration depth is seen for the cases when chirps are used in transmit. The row

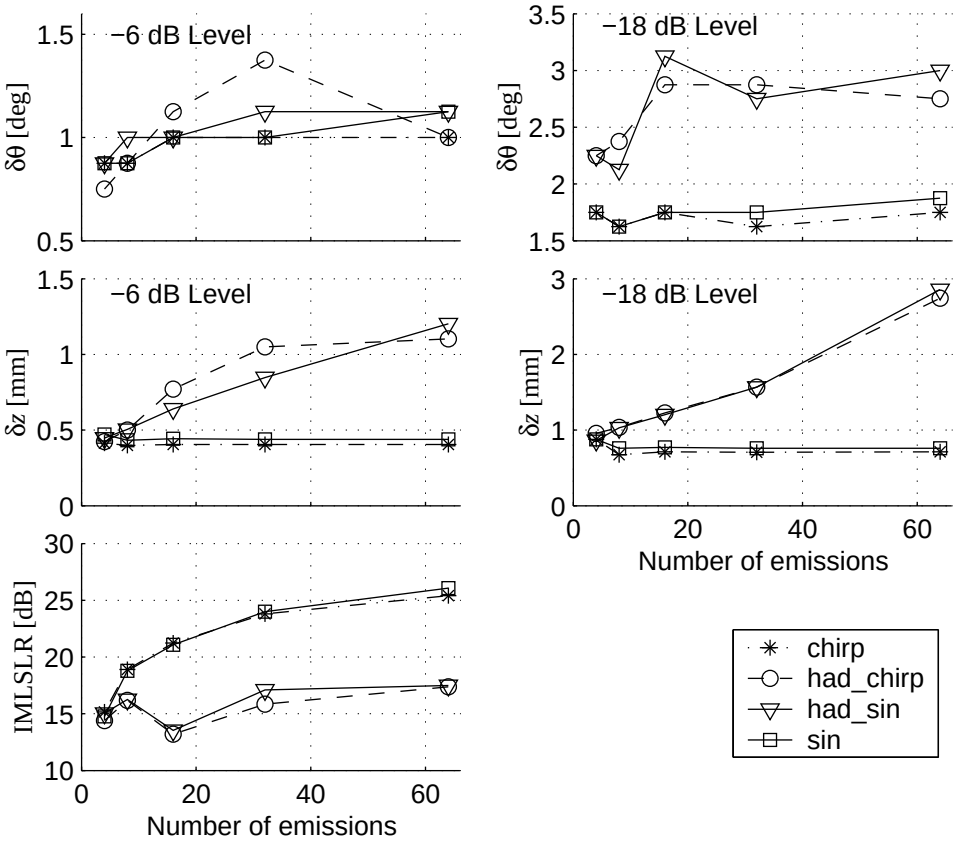


Figure 5. Comparison between some parameters of the point spread functions obtained using the different methods.

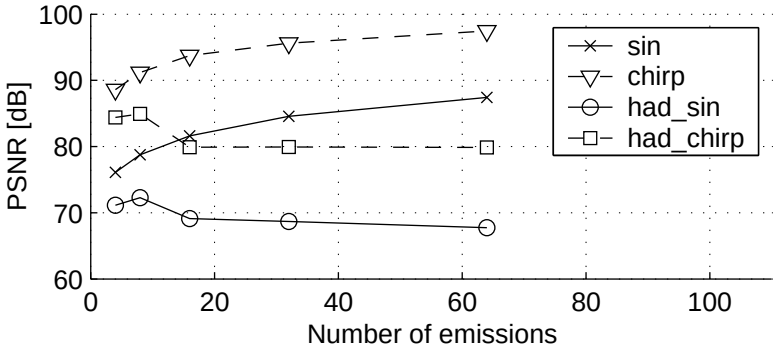


Figure 6. The peak signal to noise ratio for the various encoding schemes.

of points at 82 mm is clearly observed in both images, with, and without Hadamard encoding. The best image quality in terms of contrast, penetration depth and resolution is obtained with the combination of spatial and temporal encoding.

### 3.4 In-vivo Results

The final test for an imaging modality is its quality *in-vivo*. The experiments on wires, and on a tissue mimicking phantom showed that the synthetic aperture imaging is a viable imaging modality, and that the use of coding in space and time can increase the penetration depth, and the signal to noise ratio. The remaining question is whether the motion in the body will prevent the improvement in image quality.

| Transmit | $\delta_{\theta 6\text{dB}}$ [deg] | $\delta_{\theta 12\text{dB}}$ [deg] | $\delta_{\theta 18\text{dB}}$ [deg] | $\delta_{\theta 30\text{dB}}$ [deg] | $\delta_{z 6\text{dB}}$ [mm] | $\delta_{z 12\text{dB}}$ [mm] | $\delta_{z 18\text{dB}}$ [mm] | $\delta_{z 30\text{dB}}$ [mm] | IMLSLR [dB] |
|---|---|---|---|---|---|---|---|---|---|
| chirp_04 | 0.88 | 1.25 | 1.75 | 3.13 | 0.41 | 0.65 | 0.88 | 1.19 | 15.17 |
| chirp_08 | 0.88 | 1.25 | 1.63 | 3.38 | 0.40 | 0.54 | 0.67 | 0.93 | 18.91 |
| chirp_16 | 1.00 | 1.25 | 1.75 | 3.38 | 0.40 | 0.54 | 0.71 | 1.06 | 21.24 |
| chirp_32 | 1.00 | 1.25 | 1.63 | 3.50 | 0.40 | 0.54 | 0.71 | 1.03 | 23.80 |
| chirp_64 | 1.00 | 1.38 | 1.75 | 3.38 | 0.40 | 0.55 | 0.71 | 1.03 | 25.41 |
| had_chirp_04 | 0.75 | 1.75 | 2.25 | 3.25 | 0.42 | 0.59 | 0.96 | 1.69 | 14.40 |
| had_chirp_08 | 0.88 | 1.50 | 2.38 | 3.75 | 0.50 | 0.87 | 1.03 | 1.39 | 16.18 |
| had_chirp_16 | 1.13 | 2.38 | 2.88 | 6.88 | 0.77 | 1.01 | 1.23 | 2.07 | 13.20 |
| had_chirp_32 | 1.38 | 2.00 | 2.88 | 4.13 | 1.04 | 1.39 | 1.57 | 2.13 | 15.84 |
| had_chirp_64 | 1.00 | 2.00 | 2.75 | 4.75 | 1.10 | 2.33 | 2.74 | 3.11 | 17.37 |
| had_sin_04 | 0.88 | 1.75 | 2.25 | 3.25 | 0.45 | 0.68 | 0.86 | 1.69 | 15.04 |
| had_sin_08 | 1.00 | 1.50 | 2.13 | 3.75 | 0.51 | 0.82 | 1.03 | 1.37 | 16.26 |
| had_sin_16 | 1.01 | 2.38 | 3.13 | 6.25 | 0.64 | 1.04 | 1.20 | 1.70 | 13.54 |
| had_sin_32 | 1.13 | 1.88 | 2.75 | 3.88 | 0.85 | 1.40 | 1.57 | 1.94 | 17.09 |
| had_sin_64 | 1.13 | 2.13 | 3.00 | 5.75 | 1.20 | 2.51 | 2.86 | 3.36 | 17.49 |
| sin_04 | 0.88 | 1.25 | 1.75 | 3.38 | 0.47 | 0.71 | 0.88 | 1.20 | 14.77 |
| sin_08 | 0.88 | 1.25 | 1.63 | 3.50 | 0.43 | 0.61 | 0.76 | 1.09 | 18.78 |
| sin_16 | 1.00 | 1.50 | 1.75 | 3.63 | 0.44 | 0.62 | 0.77 | 1.18 | 21.08 |
| sin_32 | 1.00 | 1.50 | 1.75 | 3.63 | 0.44 | 0.61 | 0.76 | 1.18 | 23.99 |
| sin_64 | 1.13 | 1.38 | 1.88 | 3.63 | 0.44 | 0.61 | 0.76 | 1.19 | 26.07 |

Table 3. Resolution and IMLSLR

Figure 8 shows several B-mode images of the carotid artery. The images in the top row were obtained without the use of any codes, and in the bottom one with spatial Hadamard encoding. The vessel is too close to the surface for the chirps to be efficient, as it can be seen from the middle row. By means of simple visual inspection it can be seen that the contrast in the images increases with the increasing number of emissions. This means that for the depicted case, the motion artifacts do not influence the coherent summation to an degree, at which the image quality would decrease with increasing number of emissions.

## 4. CONCLUSIONS

A comparison between 3 different encoding schemes was made. Characterizing the point spread function using pulse echo measurements in a water bath showed that there is almost no penalty when linear FM pulses are used in transmit, and that the gain in signal to noise ratio can be more than 10 dB. Although the use of spatial encoding with Hadamard matrices showed better image quality in a tissue mimicking phantom, and *in-vivo*, a word of caution must be raised since non-linearities in the imaging process can prevent the correct reconstruction of the signals. The complexity of the system is increased significantly, and is not matched by a proportional increase in the image quality.

A clinical example of a scan of the carotid artery showed that the motion artifacts do not influence the synthetic aperture focusing significantly, and that a fairly large amount of emissions (64) can be used to form a

| | 4 | 8 | 16 | 32 | 64 |
|---|---|---|---|---|---|
| sin | 76.12 | 78.75 | 81.62 | 84.55 | 87.48 |
| chirp | 88.59 | 91.20 | 93.74 | 95.60 | 97.47 |
| had_sin | 71.14 | 72.27 | 69.11 | 68.67 | 67.75 |
| had_chirp | 84.40 | 84.94 | 79.89 | 79.93 | 79.87 |

Table 4. The peak signal to noise ratio as a function of encoding type and number of emissions. The PSNR is given in dB.

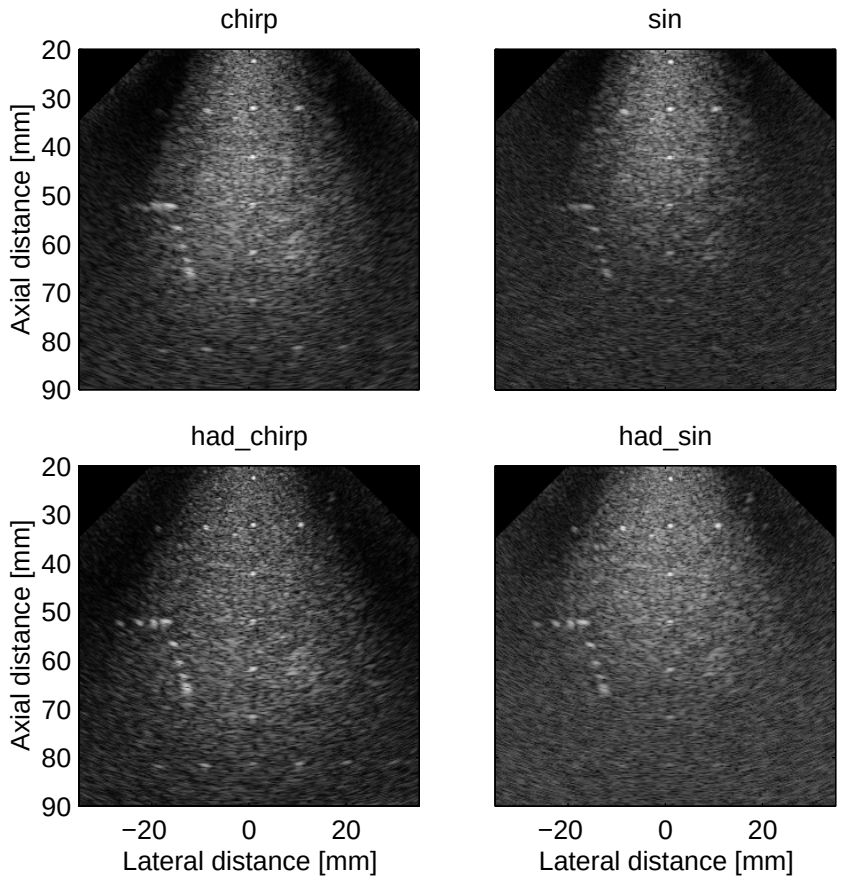


Figure 7. Measurements on a phantom using 1.5 cycles RF pulse at 7.5 MHz, 30 $\mu$s chirp, Hadamard encoding with the 1.5 cycles pulse, and Hadamard encoding with the chirp. The number of transmitting elements $N_{xmt}$ is 64 for all cases.

single frame. Both chirps and Hadamard encoding can be used in-vivo to increase the penetration depth of the scans.

## ACKNOWLEDGMENTS

This work was supported by grant 9700883 and 9700563 from the Danish Science Foundation and by B-K Medical A/S, Gentofte, Denmark.

The authors thank to Thanassis Misaridis and Kim Gammelmark for their help in the design of chirps.

## REFERENCES

1. S. Bennett, D. K. Peterson, D. Corl, and G. S. Kino. A real-time synthetic aperture digital acoustic imaging system. In P. Alais and A. F. Metherell, editors, *Acoust. Imaging*, volume 10, pages 669–692, 1982.
2. M. Karaman, P. C. Li, and M. O'Donnell. Synthetic aperture imaging for small scale systems. *IEEE Trans. Ultrason., Ferroelec., Freq. Contr.*, 42:429–442, 1995.
3. L. F. Nock and G. E. Trahey. Synthetic receive aperture imaging with phase correction for motion and for tissue inhomogenities - part I: basic principles. *IEEE Trans. Ultrason., Ferroelec., Freq. Contr.*, 39:489–495, 1992.
4. L. F. Nock and G. E. Trahey. Synthetic receive aperture imaging with phase correction for motion and for tissue inhomogenities - part I: basic principles. *IEEE Trans. Ultrason., Ferroelec., Freq. Contr.*, 39:489–495, 1992.

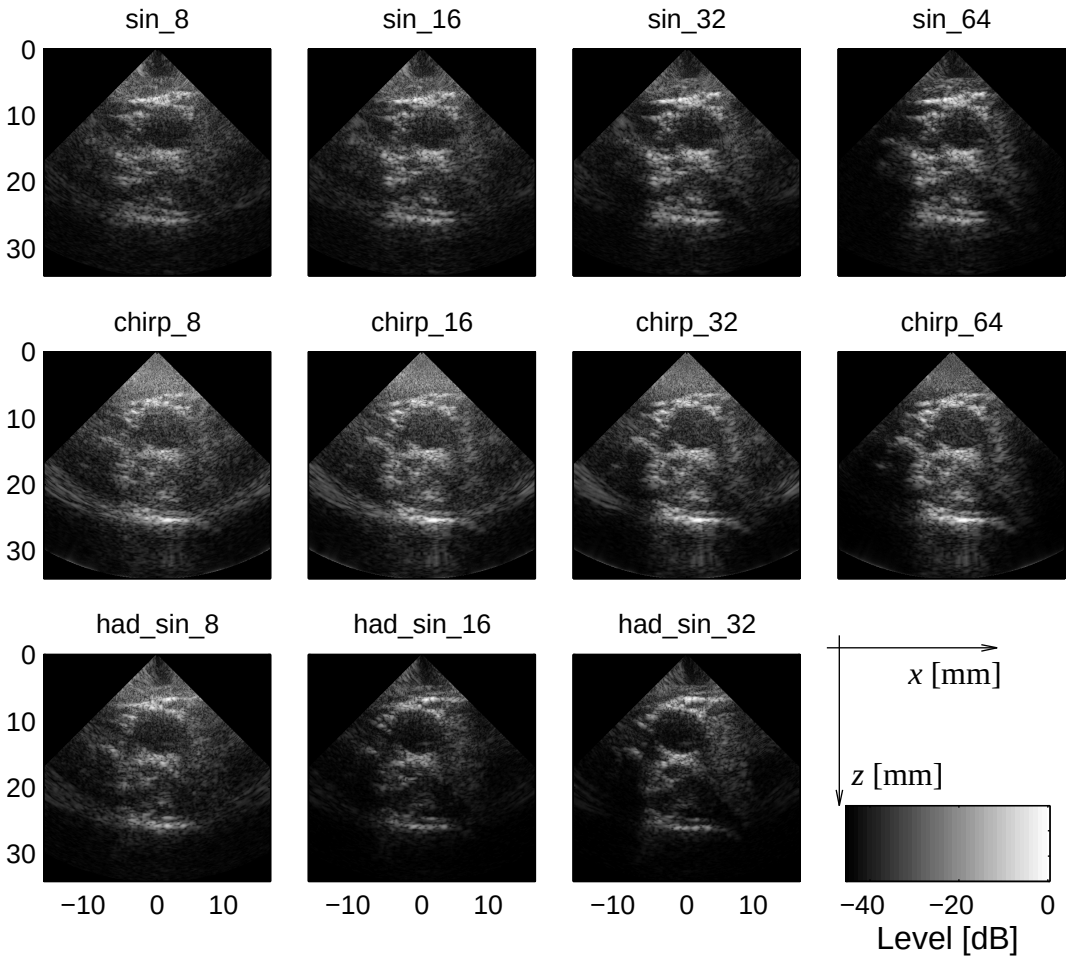


Figure 8. Measurements of the carotid artery using 1.5 cycles RF pulse at 7.5 MHz, 30 $\mu$s chirp, and Hadamard encoding with the 1.5 cycles pulse.


5. M. O'Donnell and L. J. Thomas. Efficient synthetic aperture imaging from a circular aperture with possible application to catheter-based imaging. *IEEE Trans. Ultrason., Ferroelec., Freq. Contr.*, 39:366–380, 1992.
6. M. H. Bae, M. K. Jeong, T. K. Song, and Y. B. Ahn. Experimental study of transmit synthetic focusing combined with receive dynamic focusing in B-mode ultrasound imaging systems. In *Proc. IEEE Ultrason. Symp.*, pages 1261–1264, 1999.
7. G. R. Lockwood, J. R. Talman, and S. S. Brunke. Real-time 3-D ultrasound imaging using sparse synthetic aperture beamforming. *IEEE Trans. Ultrason., Ferroelec., Freq. Contr.*, 45:980–988, 1998.
8. S. I. Nikolov, K. Gammelmark, and J. A. Jensen. Recursive ultrasound imaging. In *Proc. IEEE Ultrason. Symp.*, volume 2, pages 1621–1625, 1999.
9. S. I. Nikolov and J. A. Jensen. Velocity estimation using synthetic aperture imaging. In *Proc. IEEE Ultrason. Symp.*, pages 1409–1412, 2001.
10. S. I. Nikolov. *Synthetic Aperture Tissue and Flow Ultrasound Imaging*. PhD thesis, Ørsted•DTU, Technical University of Denmark, 2800, Lyngby, Denmark, 2001.
11. J. T. Ylitalo. On the signal-to-noise ratio of a synthetic aperture ultrasound imaging method. *Eur. J. Ultrasound*, 3:277–281, 1996.
12. S. I. Nikolov, K. Gammelmark, and J. A. Jensen. Velocity estimation using recursive ultrasound imaging and spatially encoded signals. In *Proc. IEEE Ultrason. Symp.*, volume 2, pages 1473–1477, 2000.

13. T. X. Misaridis, M. H. Pedersen, and J. A. Jensen. Clinical use and evaluation of coded excitation in B-mode images. In *Proc. IEEE Ultrason. Symp.*, volume 2, pages 1689–1693, 2000.
14. R. Y. Chiao, L. J. Thomas, and S. D. Silverstein. Sparse array imaging with spatially-encoded transmits. In *Proc. IEEE Ultrason. Symp.*, pages 1679–1682, 1997.
15. R. Y. Chiao and L. J. Thomas. Synthetic transmit aperture using orthogonal golay coded excitation. In *Proc. IEEE Ultrason. Symp.*, pages 1469–1472, 2000.
16. J. A. Jensen, O. Holm, L. J. Jensen, H. Bendsen, H. M. Pedersen, K. Salomonsen, J. Hansen, and S. Nikolov. Experimental ultrasound system for real-time synthetic imaging. In *Proc. IEEE Ultrason. Symp.*, volume 2, pages 1595–1599, 1999.
17. M.-K. Jeong, K.-J. Lee, M.-H. Bae, S.-Y. Chang, and S.-B. Gye. Beamforming using the synthetic sinc wave for ultrasonic imaging system. In *Proc. IEEE Ultrason. Symp.*, volume 2, pages 1539 – 1542, 2001.
18. M. Schlaikjer, S. Torp-Pedersen, J. A. Jensen, and P. F. Stetson. Tissue motion in blood velocity estimation and its simulation. In *Proc. IEEE Ultrason. Symp.*, pages 1495–1499, 1998.
19. T. X. Misaridis, K. Gammelmark, C. H. Jørgensen, N. Lindberg, A. H. Thomsen, M. H. Pedersen, and J. A. Jensen. Potential of coded excitation in medical ultrasound imaging. *Ultrasonics*, 38:183–189, 2000.
20. T. Misaridis. *Ultrasound imaging using coded signals.* PhD thesis, Ørsted•DTU, Technical University of Denmark, Lyngby, Denmark, 2001.